

Recoverable strain from reverse plasticity

Henry A. Lockwood and Suzanne M. Fielding¹

¹*Department of Physics, Durham University, Science Laboratories, South Road, Durham DH1 3LE, UK*

Recoverable strain is the strain recovered once a stress is removed from a body, in the direction opposite to that in which the stress had acted. To date, the phenomenon has been understood as being elastic in origin: polymer chains stretched in the direction of an imposed stress will recoil after the stress is removed, for example. Any unrecoverable strain is instead attributed to irreversible plastic deformations. Here we study theoretically recoverable and unrecoverable strain within the soft glassy rheology model, aimed at describing the rheology of elastoplastic yield stress fluids and amorphous soft solids. We consider a material subject to the switch-on of a shear stress that is held constant before later being set back to zero, after which the strain recovery is observed. After an initially fast recoil that is indeed elastic in nature, consistent with the usual intuition, we find that significant subsequent strain recovery then arises *not via further recoil of elasticity but instead by ‘reverse plasticity’*, in a sense that we discuss carefully. Also unexpectedly, although in rare parameter regimes, this plastic part of the strain post switch-off does not always in fact recover in the negative direction, counter to that of the previously imposed stress, but can sometimes continue to accumulate in the forward direction. The recovery is then non-monotonic overall, reminiscent of recent observations of non-monotonic stress relaxation after straining, which have been attributed to complex material memory effects. We elucidate the mechanisms underlying these behaviours in terms of the evolution of the SGR model’s population of elastoplastic elements, and suggest connections with the notion of ‘reversible plasticity’, as discussed in the recent physics literature.

I. INTRODUCTION

The concept of recoverable strain has a long history in the rheology literature. Reiner noted that, when stresses are removed from a body, part of the deformation will in general be recovered, and that this part of the deformation is elastic [1]. Weissenberg suggested that the stress in a flowing material can be expressed at any time in terms of a strain that relates the current state of the material to some reference state; and that this reference state, which depends on the flow history, defines the recoverable state to which the material would ultimately deform if the stress were then removed [2]. In essence, then, recoverable strain is the amount of strain recovered once a stress is removed from a body, in the direction opposite to that in which the stress had acted.

In physical terms, recoverable strain has to date been understood as elastic in origin: polymer chains elastically stretched in the direction of an imposed stress show viscoelastic recoil after the stress is removed, for example. (In a material with a single Maxwell relaxation timescale, this recovery is predicted to occur instantaneously. A superposition of Maxwell modes with distinct relaxation timescales confers a finite recovery time [3].) Indeed, the term ‘elastic recovery’ has often been used synonymously with ‘strain recovery’ [3–6]. Any unrecoverable strain is instead attributed to irreversible plastic deformations.

The same distinction is also evident in more recent literature concerning the use of recoverable vs unrecoverable strain to characterise yielding [7–10]. Donley et al. [7] note that zero-stress recovery tests allow materials to recover their instantaneous ‘ground state’, enabling calculation of the relative amounts of viscosity and elasticity. Shim and Rogers [8] state that ‘the recoverable and unrecoverable [strain] components can be interpreted

as the contributions from the viscoelastic solid and plastic properties respectively’. Kamani et al. [9] note that ‘the recoverable [strain] component is related to elastic processes, while the unrecoverable component is related to the plastic behaviour’ and that ‘yield stress fluids change from being viscoelastic solids, where deformations are recoverable, to deforming plastically, where deformation is unrecoverable’. Lee et al. [10] state that ‘recoverable strain is elastic, while viscous properties are dictated by the rate at which strain is acquired unrecoverably’.

In experimental studies, strain recovery following an initial forward creep under an imposed stress, after the stress is subsequently switched-off, has been observed in cold set gels [11], protein gels [12], fractal colloidal gels [13], hectorite clay [14], peptide gels [15], carbopol [16] and polystyrene aggregate concrete [17]. A high degree of recovery after a large deformation has been discussed as being an important property of tough hydrogels [18–21]. Shape memory effects in self-healing polymers are also attracting increasing attention [22], although here the recovery is typically induced by a change in temperature, or other control parameter besides stress or strain, which we do not consider here.

In this work, we study theoretically recoverable and unrecoverable strain within the class of materials that are variously (in different parts of the literature) referred to as soft glassy materials [23, 24], amorphous materials [25], yield stress fluids [26] or elastoplastic materials [27]. These include dense foams and emulsions, glassy colloidal suspensions, jammed athermal suspensions and granular matter, as well as harder metallic and molecular glasses. We do so by performing simulations within the widely used soft glassy rheology model [23, 24], focusing in particular on the simple recovery protocol in which a material of age t_w is subject to the switch-on at

some time zero of a shear stress of amplitude σ_0 , which is held constant until it is later set back to zero at some time t_{stop} , after which the strain recovery is observed as a function of the time $t - t_{\text{stop}}$.

Counterintuitively, we find that a significant component of strain recovery post switch-off arises not via the recoil of elasticity, but instead by *reverse plasticity*, in a sense that we discuss carefully. This observation holds robustly across broad parameter regimes. Unexpectedly – although in relatively rare parameter regimes – we also find that the plastic strain post switch-off does not always recover in the negative direction, counter to that of the originally imposed stress, but can sometimes continue to accumulate in the forward direction. The recovery process is then non-monotonic overall, with the initially backward elastic recoil followed by a (lesser) forward plastic straining. This is reminiscent of recent observations of non-monotonic stress relaxation after straining [28–31], which have been attributed to complex material memory effects [32]. We provide a mechanistic understanding of these observations in terms of the evolution of the SGR model’s population of elastoplastic elements. We also discuss possible connections with the concept of *reversible plasticity*, which has gained increasing attention in the recent physics literature.

Indeed, a key concept in the rheology of amorphous materials is that of intermittent local plastic events, sometimes called T1 events, arising at soft spots or shear transformation zones [25], coupled by elastic stress propagation [33]. Within this framework, oscillatory shear experiments on jammed particle rafts identified three different regimes of imposed strain amplitude [34–36]. At low amplitudes, the material responds elastically, with no plastic events. At high amplitudes, irreversible plastic events occur within each cycle, with significant cycle-to-cycle stroboscopic changes in particle positions. More surprisingly, at intermediate strain amplitudes these experiments report *reversible local plastic events* within each cycle. Such events dissipate energy, consistent with the notion of plasticity, *but exactly reverse in the opposite part of the cycle, with zero stroboscopic cycle-to-cycle change in particle positions*. Reversible plastic events have also been reported in experiments on foams [37], in particle simulations [37–41] and in elastoplastic models [42]. Reversible plastic limit cycles have likewise been studied in models of hysterons [43] and iterated maps [44]. For a review, see Ref. [45].

The paper is structured as follows. In Sec. II we outline the SGR model [23, 24], within which we shall study the phenomenon of strain recovery. The step stress protocol that we shall simulate is specified in Sec. III. In Sec. IV we define our units, summarise the parameters of the model and protocol, and discuss the rheological quantities to be measured. Our results are presented in Sec. V. We set out our conclusions in Sec. VI.

II. SOFT GLASSY RHEOLOGY MODEL

The soft glassy rheology (SGR) model [23, 24] considers the dynamics of an ensemble of elastoplastic elements that explore a landscape of energy traps. Each element is notionally taken to represent a local mesoscopic region of a soft glassy material: a few tens of droplets in a dense emulsion, for example. Each element is assumed small relative to any macroscopic variations in the flow field, on the one hand, yet large enough to allow the definition of local continuum variables of shear strain l and shear stress kl , on the other. The local strain variable l is taken to describe the element’s state of elastic deformation relative to a locally undeformed equilibrium. Between local plastic yielding events, defined below, the strain of each element is assumed elastically to follow the macroscopically imposed strain rate $\dot{\gamma}$, such that $\dot{l} = \dot{\gamma}$.

Plasticity is incorporated by assuming that these local stresses are intermittently released by local plastic yielding events. In each such yielding event, a mesoscopic region of material is assumed suddenly to rearrange itself into a new local configuration, relative to a new state of local equilibrium. This is modelled by the corresponding representative elastoplastic element hopping between traps in the model’s energy landscape: at any instant in time, an element that lies in a trap of energy depth E and has local shear strain l is assumed to have a probability per unit time of hopping given by

$$r(E, l) = \tau_0^{-1} \max \left\{ 1, \exp \left[\left(\frac{1}{2} kl^2 - E \right) / x \right] \right\}, \quad (1)$$

with τ_0 a microscopic attempt time. As can be seen via this expression, the elastic strain energy $\frac{1}{2} kl^2$ essentially reduces the local energy barrier E , giving an effective barrier $E - \frac{1}{2} kl^2$. This shear-induced reduction in barrier heights renders the model’s overall rheological behaviour shear thinning. Depending on the material considered, the parameter x can be interpreted as the true thermal temperature or an effective noise temperature: a point to which we shall return below.

After hopping, an element is assumed instantaneously to select a new trap depth randomly from the landscape’s prior distribution of trap depths, taken to be of the form:

$$\rho(E) = \frac{1}{x_g} \exp(-E/x_g), \quad (2)$$

in which x_g is the model’s glass transition (effective) temperature, discussed further below. The element is further assumed to reset its local strain l to zero, so relaxing its stress. (Post-hop frustration can be incorporated by assuming a post-hop strain distribution of non-zero width, though we do not consider that here.)

With these dynamics, the joint probability $P(E, l, t)$ for an element to be found at any time t in a trap of depth E , and with local shear strain l , evolves via the following master equation:

$$\dot{P}(E, l, t) + \dot{\gamma} \frac{\partial P}{\partial l} = -r(E, l)P + Y(t)\rho(E)\delta(l). \quad (3)$$

The advection term on the left hand side captures the elastic loading of each element within its trap. The first term on the right hand side describes the local plastic relaxation events described above. Because these are modelled by hops out of traps, this takes the form of a ‘death’ term. The second term on the right hand side is a ‘re-birth’ term, describing the hopping of freshly yielded elements into the bottom of new traps, $l = 0$, with the new trap depth selected randomly from the prior $\rho(E)$ of Eqn. 2. The ensemble average hopping rate

$$Y(t) = \int dE \int dl r(E, l) P(E, l, t), \quad (4)$$

and the ensemble average macroscopic stress

$$\sigma(t) = k \int dE \int dl l P(E, l, t). \quad (5)$$

In combination with the exponential prior distribution of trap depths across the model’s energy landscape, $\rho(E)$, the exponential activation factor $r(E, l)$ confers a glass transition at an effective temperature $x = x_g$. In the absence of any imposed shear, the model captures rheological ageing for effective temperatures in the glass phase $x < x_g$ [46]. Following the preparation of a sample via a sudden quench from a high initial effective temperature to a working temperature $x < x_g$, the system slowly evolves into ever deeper traps as a function of the time since the temperature quench. The overall stress relaxation time grows linearly with time, giving progressively more solid-like rheology as the sample ages.

Conversely, an imposed shear of rate $\dot{\gamma}$ will halt this ageing process and rejuvenate the sample to a flowing state with an effective age set by the inverse shear rate, $1/\dot{\gamma}$. In its glass phase, $x < x_g$, the model predicts steady state flow curves with a yield stress $\sigma_Y(x)$ in the limit of slow shear $\dot{\gamma} \rightarrow 0$. For $x_g < x < 2x_g$ the model predicts power law flow curves with a shear-thinning (sublinear) exponent, giving infinite viscosity in the limit of slow shear. For $x > 2x_g$, the flow curves are Newtonian.

In many soft glassy materials, the typical scale of energy barriers for local rearrangement events – the penalty for stretching soap films in a foam, for example – is far greater than the typical scale of thermal energy, $k_B T$. In such materials, the parameter x is taken to be an effective noise temperature that models an assumed coupling with other yielding events elsewhere in the sample. This is intended to capture in a mean-field way the basic idea that a local yielding event in one part of the sample may trigger follow-on yielding events in other regions. To date, this remains a mean-field assumption that is yet to be made self consistent. In materials for which the energy barriers are instead on the scale of $k_B T$, the parameter x can be taken as the true thermal temperature.

III. PROTOCOL

In this section, we define the recovery protocol that we shall simulate within the SGR model just described.

Sample preparation prior to shear is modelled by assuming a sudden deep quench at some time $t = -t_w$, from infinite effective temperature to the final working value x , which is held constant thereafter. For times $-t_w < t < 0$ the sample is allowed to age undisturbed, without any strain or stress being applied. Throughout most of the paper, we assume that all elemental strains are equal to zero during this initial ageing stage, $l = 0$. An exception can be found in Figs. 3 and 4, where we assume an initial Gaussian distribution of l values, of narrow standard deviation $l_0 = 0.05$. This does not affect the basic physics of interest in this work, but merely allows us to show as a narrow Gaussian in Fig. 4 what would otherwise be an unplotable initial delta function distribution.

At time $t = 0$, a step stress of amplitude σ_0 is imposed. At the time of this step, all elements instantaneously strain elastically forward within their traps by the same amount $l = \sigma_0/k$, giving an instantaneous global elastic strain response $\gamma_0 = \sigma_0/k$. With the imposed stress held constant and equal to σ_0 , we then allow the sample to strain further forward by an amount $\Delta\gamma_f$, beyond the elastic straining that occurred at the instant the stress was imposed. Note that this further straining arises from elements hopping between traps, and accordingly is plastic in nature. Once the total strain has attained a value $\gamma(t) = \gamma_0 + \Delta\gamma_f$, we set the stress to zero, $\sigma = 0$. We define the time at which this occurs as $t = t_{\text{stop}}$. In principle, we could use either t_{stop} or $\Delta\gamma_f$ as a control parameter in our study. In practice, we have chosen to use $\Delta\gamma_f$ because it better reflects the physical state of the material at switch-off.

For all subsequent times, $t > t_{\text{stop}}$, we hold the stress equal to zero and measure the strain γ as a function of the time interval $t - t_{\text{stop}}$ since switch-off. We shall be interested in particular in the degree to which the strain recovers in the negative direction, whether it does so monotonically or non-monotonically, and in the basic physics that underlies this recovery process.

IV. UNITS, PARAMETER VALUES AND MEASURED QUANTITIES

The parameters of the SGR model are the effective temperature x , the attempt time for local yielding events τ_0 , the elemental modulus k , and the glass transition temperature x_g . Recall Sec. II. The parameters of the rheological protocol are the time t_w for which the sample is aged before the stress is imposed, the amplitude of the imposed stress σ_0 , and the degree to which the sample is allowed to strain further forwards due to plastic yielding while the stress is held fixed, $\Delta\gamma_f$. Recall Sec. III.

To solve the SGR model numerically, we simulate a population of M SGR elements. In any timestep dt , any element is hopped with probability $r dt$, with r that element’s probability per unit time of hopping as given by Eqn. 1 above.

We work in units of stress in which the modulus $k = 1$,

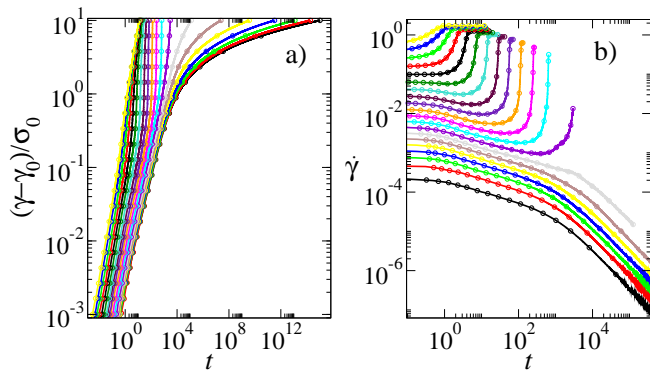


FIG. 1. Forward strain evolution during stress application. **a)** Plastic strain $\gamma(t) - \gamma_0$ as a function of time t after the initial elastic step of size γ_0 that arises at the instant of switch-on at $t = 0$, normalised by the amplitude of the imposed stress σ_0 . **b)** Corresponding strain rate as a function of time. Waiting time $t_w = 10^3$. Imposed stress $\sigma_0 = 0.1, 0.2 \dots 2.0$ in curves upwards. Dots are placed at equally logarithmically spaced values of the scaled strain for each imposed stress value in **a)**, and at corresponding times in **b)**.

and of time in which $\tau_0 = 1$. We restrict ourselves to homogeneous shear, assuming that (for example) no shear bands form either during forward creep or backward recovery. With this simplification, there is no lengthscale implied by the flow geometry or model. We also set the glass transition temperature $x_g = 1$. This amounts to setting the average trap depth in the landscape's prior distribution to unity, thereby setting the typical scale of *strain* for local yielding events. To compare with any experimental data, therefore, all strains reported below would need to be rescaled by the typical strain for local yielding events in the material.

We set the noise temperature $x = 0.3$, deep within the glass phase. Results are presented for a number of SGR elements $M = 10^5$, convergence checked against $M = 10^6$. The numerical timestep $dt = \alpha / \langle |l| r(E, l) \rangle$ with $\alpha = 10^{-5}$, convergence checked against $\alpha = 2 \times 10^{-6}$.

Important physical parameters to be explored are then the sample age t_w prior to stress switch-on, the amplitude of the imposed stress σ_0 , and the degree of forward plastic strain that accumulates before the stress is switched off, $\Delta\gamma_f$. Recall from Sec. IV that this further defines a switch-off time $t_{\text{stop}}(x, t_w, \sigma_0, \Delta\gamma_f)$.

At the instant of stress switch-off, all elements instantaneously strain elastically backwards, giving a global strain change $\Delta\gamma = -\sigma_0$ (in our units). We then measure the subsequent strain evolution as a function of the time $t - t_{\text{stop}}^+$ since switch-off. Our interest in particular will be in the total reverse strain $\Delta\gamma_{\text{rec}}$ accumulated in the long time limit, $t - t_{\text{stop}} \rightarrow \infty$, beyond that which arose elastically during the reverse step. As noted above, in rare cases we shall find $\Delta\gamma_{\text{rec}} < 0$: the plastic straining after the initial reverse elastic recoil in fact takes place in the forward direction.

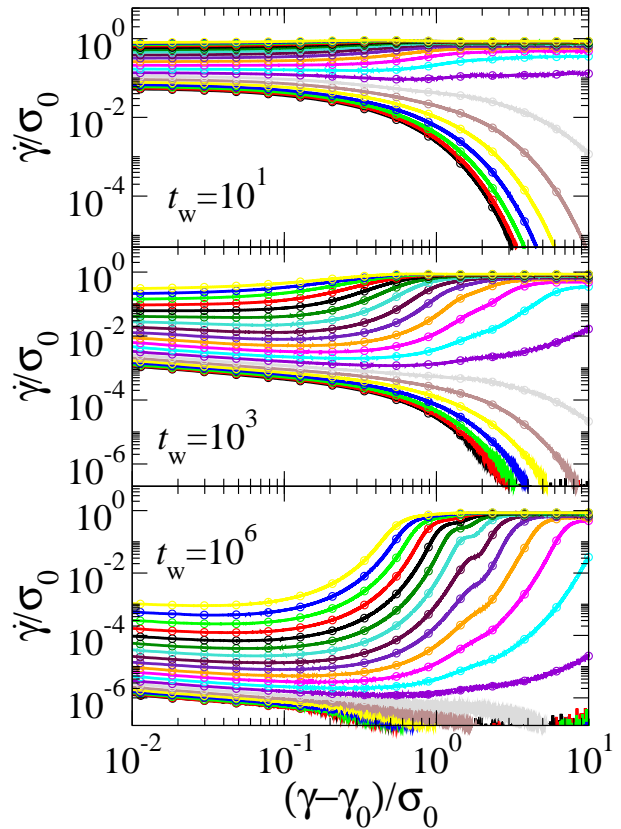


FIG. 2. Forward strain evolution during stress application. The strain rate is normalised by the imposed stress and parametrically plotted as a function of the plastic strain that arises beyond the initial elastic step strain, also normalised by the imposed stress. Imposed stress $\sigma_0 = 0.1, 0.2 \dots 2.0$ in curves upwards in each panel. Waiting time $t_w = 10^1, 10^3$ and 10^6 indicated in each panel. Dots show equally logarithmically spaced values of the scaled forward plastic strain $(\gamma - \gamma_0)/\sigma_0 = \Delta\gamma_f/\sigma_0$ for which the subsequent strain recovery after switch-off is reported in Fig. 5.

V. RESULTS

We now present our results. As a preamble to understanding strain recovery post switch-off, we shall start in Sec. VA by analysing the forward creep and/or yielding and flow that arise while the stress is held imposed. We then present our results for strain recovery in Sec. VB.

A. Forward strain during stress application

Following the application of a step stress of magnitude σ_0 at time $t = 0$, a material's creep response is characterised by the strain curve $\gamma(t)$. As noted above, in the SGR model this shows an initially elastic step strain of magnitude $\gamma_0 = \sigma_0/k$ ($= \sigma_0$ in our units) at $t = 0$, followed by subsequent plastic straining for $t > 0$. Fig. 1a) shows this plastic part of the creep, beyond the initial

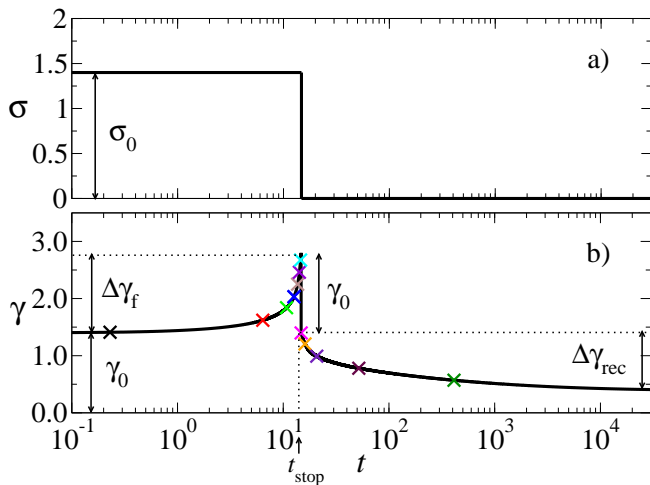


FIG. 3. **a)** Imposed stress σ as a function of time t . The sample is prepared at time $t = -t_w$ via a deep temperature quench, then left to age undisturbed for a time t_w (not shown). At time $t = 0$ a stress of amplitude σ_0 is imposed and held constant until a time t_{stop} (defined below). The stress is then set to zero and held at zero for all times $t > t_{\text{stop}}$.

b) Strain response $\gamma(t)$. At the instant the stress is imposed, $t = 0$, the system shows an instantaneous forward elastic step strain of amplitude $\gamma_0 = \sigma_0$ (in our units). The strain then subsequently increases beyond γ_0 due to plastic yielding events. Once it has done so by an amount $\Delta\gamma_f$, the stress is set back to zero. This defines the switch-off time t_{stop} . At this instant $t = t_{\text{stop}}$, the system shows an instantaneous backward elastic step strain of amplitude γ_0 . The strain then subsequently further recovers in the negative direction (usually) by an additional amplitude $\Delta\gamma_{\text{rec}}$. Parameters: $x = 0.3$, $\sigma_0 = 1.4$, $t_w = 10^3$, $\Delta\gamma_f = 1.4$.

elastic step, normalised by the stress amplitude σ_0 . Results are shown for a fixed sample age t_w , and several imposed stresses in curves upwards. The corresponding strain rate curves $\dot{\gamma}(t)$ are shown in panel b).

For the noise temperature explored here, $x = 0.3$, deep within the glass phase, the SGR model's yield stress $\sigma_Y \approx 0.748$. For imposed stresses $\sigma_0 < \sigma_Y$, the strain rate decreases perpetually as a power law $\dot{\gamma} \sim t^{-\alpha}$. The exponent $0 < \alpha < 1$ depends on the noise temperature x . The strain correspondingly increases sublinearly as $\gamma \sim t^{1-\alpha}$, corresponding to sustained power-law creep. In contrast, for imposed stresses $\sigma_0 > \sigma_Y$, an initial interval of creep (for $\sigma_0 \gtrsim \sigma_Y$ at least) is interrupted by yielding, in which the strain rate curves upwards before finally settling to a time-independent value prescribed by the steady state flow curve $\sigma_{\text{ss}}(\dot{\gamma})$, with $\sigma_{\text{ss}} - \sigma_Y(x) \sim \dot{\gamma}^{1-x}$. The time delay before yielding scales as the sample age t_w , with a prefactor that diverges as $\sigma_0 - \sigma_Y \rightarrow 0^+$ [46].

Fig. 2b) shows the same data as in Fig. 1, but with the scaled strain rate $\dot{\gamma}(t)/\sigma_0$ now plotted parametrically as a function of the forward plastic strain $(\gamma(t) - \gamma_0)/\sigma_0$. Accordingly, time t is not explicitly represented in Fig. 2. The scaled strain on the abscissa however increases monotonically with increasing t . The counterpart data

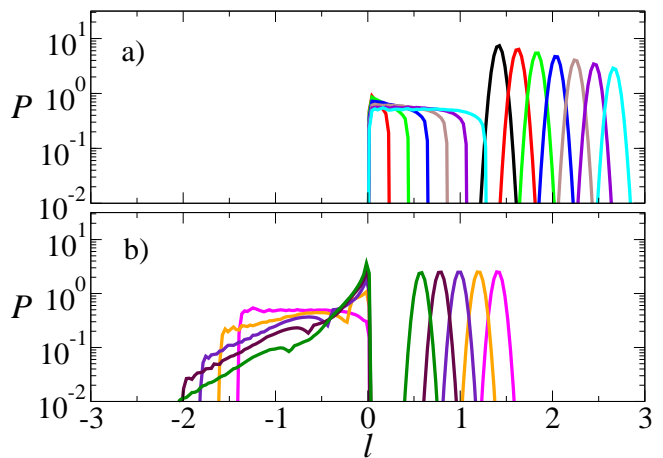


FIG. 4. Probability distribution $P(l)$ of local elemental strains at several times during the simulation of Fig. 3. **a)** While the stress is held applied, at times shown by crosses in Fig. 3, with time increasing in distributions left to right. **b)** After the stress has been switched off, at times shown by crosses in Fig. 3, with time increasing in distributions right to left. Line colours correspond to cross colours in Fig. 3.

for sample ages $t_w = 10^1$ and 10^6 are shown in Figs. 2a) and c) respectively. As can be seen, for imposed stresses above the yield stress, $\sigma_0 > \sigma_Y$, yielding typically occurs at a scaled strain $(\gamma - \gamma_0)/\sigma_0 = O(1)$, although the value increases slowly with t_w and diverges as $\sigma_0 \rightarrow \sigma_Y^+$.

A dot at each of several logarithmically spaced values of the abscissa in Fig. 2 shows the values of scaled forward plastic strain $(\gamma - \gamma_0)/\sigma_0 = \Delta\gamma_f/\sigma_0$ at which we shall later, in Fig. 5, explore the amount of strain $\Delta\gamma_{\text{rec}}$ that is ultimately recovered after the stress is switched off.

B. Strain recovery after stress switch-off

Having mapped out the forward creep and/or yielding and flow that arise while the stress is held imposed, we now explore the strain recovery after the stress is switched off. Our focus will be in particular on the part of this recovery that stems from reverse plasticity, after the initial elastic recoil at the instant of switch-off.

The basic physics that we aim to elucidate is shown in Figs. 3 and 4. The imposed stress σ as a function of time t is shown in the top panel of Fig. 3. The corresponding strain response $\gamma(t)$ is shown in the bottom panel. As described above, a stress of amplitude σ_0 is switched on at time $t = 0$. (The preparation phase during which the sample is allowed to age undisturbed for a time t_w prior to $t = 0$ is not shown.) At the instant of switch-on, the system shows an instantaneous forward elastic step strain of amplitude $\gamma_0 = \sigma_0$, in our units in which $k = 1$. (In experimental practice, this forward strain would be rapid but not instantaneous, with a rate limited by inertia or dissipation.) The stress is then held constant for some time interval, over which the strain increases further due

to plastic yielding events, this forward straining having been explored in Sec. V A. Once it has thus increased by an amount $\Delta\gamma_f$ beyond γ_0 , the stress is switched off. This defines the switch-off time t_{stop} . At the instant of switch-off, $t = t_{\text{stop}}$, the system shows an instantaneous backward elastic step strain, $\Delta\gamma = -\sigma_0 = -\gamma_0$. The stress is then held at zero for all subsequent times $t > t_{\text{stop}}$. As a function of the time interval $t - t_{\text{stop}}^+$, the strain further recovers in the negative direction by an amplitude $\Delta\gamma_{\text{rec}}$, beyond the negative elastic step $\Delta\gamma = -\gamma_0$ that occurred at the instant of switch-off. This additional recovery $\Delta\gamma_{\text{rec}}$, which has a significant amplitude compared with both $\Delta\gamma_f$ and γ_0 , arises from reverse plasticity post switch-off in a way that we shall now describe.

To understand the physics underlying this strain evolution, let us consider the master equation governing the time evolution of the joint probability distribution of elemental trap depths E and strains l . This was specified in Eqn. 3, which we repeat here for convenience:

$$\dot{P}(E, l, t) + \dot{\gamma} \frac{\partial P}{\partial l} = -r(E, l)P + Y(t)\rho(E)\delta(l). \quad (6)$$

Multiplying across by l and integrating over all l then gives a constitutive equation (albeit not in closed form) for the evolution of the stress, σ , at imposed strain rate:

$$\dot{\sigma}(t) = \dot{\gamma}(t) - \langle l r(E, l) \rangle_{P(E, l, t)}. \quad (7)$$

In this equation, the first term on the right hand side stems from the elastic loading term that describes the advection of elemental strains while elements remain in their traps. The second term stems from stress relaxation due to local plastic yielding events, as elements hop between traps. The evolution of the strain rate at an imposed stress is then of course simply:

$$\dot{\gamma}(t) = \dot{\sigma}(t) + \langle l r(E, l) \rangle_{P(E, l, t)}. \quad (8)$$

Consider the predictions of this equation for the imposed-stress protocol of interest here. Integrating across the positive (resp. negative) step in stress at $t = 0$ (resp. $t = t_{\text{stop}}$) gives an elastic step strain of the same amplitude and sign as the step stress (in our units in which $k = 1$), as indeed discussed above and seen numerically in Fig. 3.

In contrast, during any interval in which the stress is constant, $\dot{\sigma} = 0$, either while the stress of amplitude $\sigma = \sigma_0$ is held imposed, or after switch-off when $\sigma = 0$, the strain rate is given by

$$\dot{\gamma}(t) = \langle l r(E, l) \rangle_{P(E, l, t)}. \quad (9)$$

Importantly, this tells us that both the forward straining $\Delta\gamma_f$ that occurs after switch-on but before switch-off, and the reverse strain recovery $\Delta\gamma_{\text{rec}}$ that occurs after switch-off, are determined *purely by the relaxation of local stresses due to local plastic yielding events*. Indeed, as these local plastic events occur and elements hop between traps, a global straining must arise in order to

advect elements within their traps and exactly counterbalance any such plastic stress loss (or gain), keeping the overall stress constant.

In order fully to understand the forward plastic straining during stress imposition and the reverse plastic strain recovery afterwards, therefore, we must consider in more detail the evolution of the probability distribution of local strains, and the way this determines the strain rate $\dot{\gamma}(t)$ via Eqn. 9. Accordingly, we plot this distribution $P(l, t)$ in Fig. 4 (having first integrated out the trap energy depth variable E). We do so at several times t while the stress is held applied (top panel in Fig. 4), and at several times after the stress is switched off (bottom panel). The time at which any distribution is plotted in Fig. 4 is indicated by a cross of corresponding colour in Fig. 3.

The form of these distributions in Fig. 4 can be understood as follows. At the end of the sample preparation phase, immediately before the stress is applied, the distribution of local strains is (by assumption) a Gaussian of narrow width l_0 , centred at $l = 0$. (As noted above, our results in all figures except 3 and 4 have $l_0 = 0$, corresponding to a delta function.) At the instant the stress is switched on, this distribution shifts via the elastic advection term, without changing shape, to be now centred at $l = +\sigma_0 = +\gamma_0$. This distribution is shown by the black curve in Fig. 4. Over subsequent times while the stress is held imposed, plastic yielding events arise: recall that an element in a trap of depth E with local strain l has a hopping rate $r(E, l)$ given by Eqn. 1. When any such plastic event occurs, the corresponding element resets its local strain $l \rightarrow 0$. This slightly depletes the original spike in the distribution centred at $l = \sigma_0$, and leads to the development of a secondary lobe of probability around $l = 0$.

Were the strain held constant, with zero strain rate $\dot{\gamma} = 0$, the macroscopic consequence of these plastic relaxation events would be a relaxation of the ensemble average stress at rate $\dot{\sigma} = \langle l r(E, l) \rangle_{P(t)}$. Conversely, to maintain the stress constant, $\sigma = +\sigma_0$ with $\dot{\sigma} = 0$, requires a forward strain of corresponding rate $\dot{\gamma} = \langle l r(E, l) \rangle_{P(t)}$, ensuring sufficient forward advection of elements within their traps exactly to counterbalance this plastic relaxation. This is the origin of the forward plastic straining seen for times $0 < t < t_{\text{stop}}$ in Fig. 3. Its consequence is to advect forward at rate $\dot{l} = \dot{\gamma}$ both the spike in probability centred (originally) at $l = \sigma_0 = \gamma_0$ (as it simultaneously depletes due to the plastic relaxation events just described), as well as the newly developing lobe of probability near the origin $l \approx 0$. In this way, the distribution evolves over time from the black to cyan curve in the top panel of Fig. 4.

At the instant the stress is switched off, the distribution of local strains instantaneously shifts by $l \rightarrow l - \gamma_0$, with $\gamma_0 = \sigma_0$, without changing shape, as each element elastically reduces its strain within its trap. Accordingly, the rightmost (cyan) curve in the top panel of Fig. 4, which obtained at $t = t_{\text{stop}}^-$, shifts to become the rightmost (magenta) curve in the bottom panel at $t = t_{\text{stop}}^+$.

Importantly, this distribution shown in magenta just after switch-off now has some weight for strains $-\gamma_0 < l < -\gamma_0 + \Delta\gamma_f$, corresponding to those elements that had plastically yielded and reset their strains to zero while the stress was held applied, and then shifted elastically by $l \rightarrow l - \gamma_0$ at switch-off. *These elements then themselves plastically yield over the subsequent time $t - t_{\text{stop}}$ since switch-off, resetting their strains from that negative strain interval $-\gamma_0 < l < -\gamma_0 + \Delta\gamma_f$ to $l = 0$.* Accordingly, weight is progressively lost from the leftmost part of this probability lobe at negative l , with probability instead accumulating nearer $l = 0$, in moving from the magenta to green curves in the bottom panel of Fig. 4.

If the strain were held constant, the macroscopic effect of these plastic yielding events from negative to zero l would be a *positive* growth in stress, via Eqn. 9, as elements hop from negative to zero local stress. Conversely, under the conditions of constant stress that pertain after stress switch off, $\sigma = 0$ and $\dot{\sigma} = 0$, a corresponding *negative strain rate* is required to advect elements in the negative direction in their traps, in order to counterbalance this positive plastic stress change. Accordingly, as weight is lost from the negative l part of the distribution in moving from the magenta to green curves, these curves also simultaneously advect leftwards. *We therefore now understand the strain recovery that arises after stress switch-off within the SGR model to stem from these ‘reverse local plastic yielding events’.*

With this picture of the basic physics of strain recovery via reverse plasticity in mind, we shall now explore the dependence of the phenomenon on each of the three control parameters in our study: the amplitude of imposed stress σ_0 , the degree to which the sample plastically strains forward while the stress is held imposed $\Delta\gamma_f$, and the age of the sample t_w before stress switch-on. We shall consider first in Fig. 5 the total strain $\Delta\gamma_{\text{rec}}$ recovered plastically at long times $t - t_{\text{stop}} \rightarrow \infty$, before examining the time-dependence of the recovery process in Fig. 6. Recall that $\Delta\gamma_f$ and $\Delta\gamma_{\text{rec}}$ are indicated on the left and hand sides respectively of Fig. 3b): a value $\Delta\gamma_{\text{rec}} = 0$ corresponds to zero plastic strain recovery (beyond the initial elastic recoil $\Delta\gamma = -\gamma_0$ at the instant of switch-off), whereas a value $\Delta\gamma_{\text{rec}} = \Delta\gamma_f$ would indicate full recovery.

Accordingly, we plot in Fig. 5 the scaled plastic strain recovery $\Delta\gamma_{\text{rec}}/\Delta\gamma_f$ as a function of the scaled forward plastic strain $\Delta\gamma_f/\sigma_0$ that accumulated while the stress was imposed. Data are shown for imposed stress values $\sigma_0 = 0.1, 0.2 \dots 2.0$ in curves upwards in each panel, for samples ages $t_w = 10^1, 10^3$ and 10^6 in panels downwards, corresponding to the counterpart forward plastic creep curves in Fig. 2. Indeed, dots marked left to right on each creep curve in Fig. 2 show the various scaled forward strain values at switch-off, $(\gamma(t) - \gamma_0)/\sigma_0 = \Delta\gamma_f/\sigma_0$, shown as corresponding data point dots on each curve in Fig. 5.

To understand the trends observed in Fig. 5 we recall that, immediately prior to stress switch-off, any elements

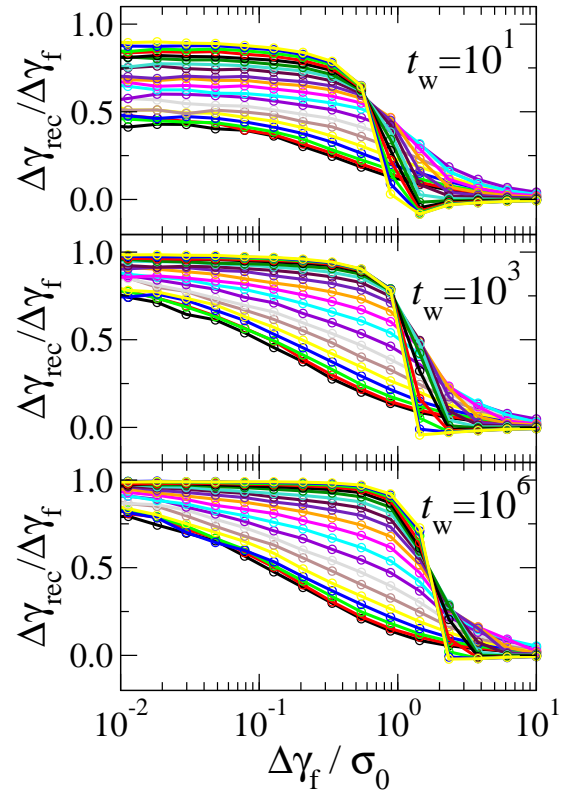


FIG. 5. Total strain plastically recovered in the reverse direction at long times $t - t_{\text{stop}} \rightarrow \infty$ after switch-off, $\Delta\gamma_{\text{rec}}$, scaled by the forward plastic strain $\Delta\gamma_f$ that arose while the stress was held imposed. Recall that a value $\Delta\gamma_{\text{rec}}/\Delta\gamma_f = 1$ would indicate full strain recovery. This normalised recovery is plotted as a function of the forward plastic strain that arose while the stress was imposed, normalised by the imposed stress. Imposed stress $\sigma_0 = 0.1, 0.2 \dots 2.0$ in curves upward in each panel. Waiting time $t_w = 10^1, 10^3$ and 10^6 indicated in each panel. Dots indicate equally logarithmically spaced values of the scaled forward plastic strain prior to switch-off, $(\gamma - \gamma_0)/\sigma_0 = \Delta\gamma_f/\sigma_0$, corresponding to the dots marked on the differentiated creep curves in Fig. 2.

that remain unyielded since the stress was imposed have local strain $l = \sigma_0 + \Delta\gamma_f$, as in the rightmost lobe of the cyan distribution in Fig. 4. (This actually has a slightly smeared distribution of strain values of small width l_0 . As noted above, this is simply for the purposes of being able to plot the distribution graphically and does not change the basic physics.) We shall call these ‘group I’ elements. In contrast, those elements that yielded at least once during the initial forward creep (‘group II’) have local strain values in the range $0 < l < \Delta\gamma_f$, giving the leftmost lobe of that distribution. At the instant of stress switch-off, the whole distribution of shifts to the left, with each $l \rightarrow l - \sigma_0$. Immediately after switch-off, therefore, the unyielded group I elements have positive local strain $l = \Delta\gamma_f$, as in the (slightly smeared) rightmost lobe of the magenta distribution in Fig. 4. They furthermore reside in traps of a depth set by the age t_w , and with

a rate of yielding $r \sim 1/t_w$. In contrast, the yielded group II elements have local strain values in the range $-\sigma_0 < l < \Delta\gamma_f - \sigma_0$ immediately post switch-off, as in leftmost lobe of the magenta distribution in Fig. 4. And in being freshly yielded, they reside in shallow traps with a rate of yielding $r = O(1)$. The relative proportion of elements in group II compared to those in group I increases with increasing forward strain $\Delta\gamma_f$.

Strain recovery post switch-off then arises from a basic competition between the plastic yielding of elements in group I versus those in group II. In most parameter regimes, the yielding of group II outweighs that of group I. When these negatively strained group II elements yield, they reset their local strains to zero. As discussed above, to maintain the stress constant and equal to zero post switch off, an exactly counterbalancing *negative* global strain - *strain recovery* - must arise.

Indeed, for small forward plastic strain values $\Delta\gamma_f < \sigma_0$, all group II elements have negative local strains post switch-off. In this regime, the larger the imposed stress σ_0 prior to switch-off, the more negative overall will be the local strains of group II elements post switch-off, requiring more counterbalancing recovery. This explains the increasing levels of recovery with increasing imposed stress prior to switch-off at the left of Fig. 5. The larger the sample age t_w , the greater the dominance of group II over group I elements, which are stuck in deep traps with yielding rate $1/t_w$. Accordingly, the degree of strain recovery increases with increasing t_w in moving from the top to the bottom panels of Fig. 5, for these small $\Delta\gamma_f/\sigma_0$.

A different trend is however observed for larger values of the scaled forward strain prior to switch-off, $\Delta\gamma_f/\sigma_0 \gtrsim 1$. In this case, for large imposed stresses, the ultimate plastic strain recovery is actually observed to be *negative*: the system strains plastically further *forwards* as a function of time $t > 0$ since switch-off. The overall strain recovery is therefore non-monotonic, with the initially backward elastic recoil at the instant of switch-off $t = t_{\text{stop}}$ followed by this forward plastic straining for $t > t_{\text{stop}}$, reminiscent of observations of non-monotonic stress relaxation after straining [28–31]. (The total recovery is still however negative, with the initial elastic recoil always exceeding any subsequent forward plastic straining, for all parameter regimes we have explored.)

This counter-intuitive observation of *forward* plastic straining post switch-off can be understood as follows. For these larger values of $\Delta\gamma_f \gtrsim \sigma_0$, the local strain distribution $-\sigma_0 < l < \Delta\gamma_f - \sigma_0$ of group II elements immediately post switch-off contains some weight at positive strain $l > 0$. Furthermore, group I elements are also strained further forwards in their traps, acquiring larger yielding rates. In consequence, as the time since switch-off elapses, the yielding of elements with positive local strains now outweighs that of elements with negative local strains. To maintain zero stress post switch-off, this must be exactly counter-balanced by an *increase* in strain, giving *negative* strain recovery. This effect is

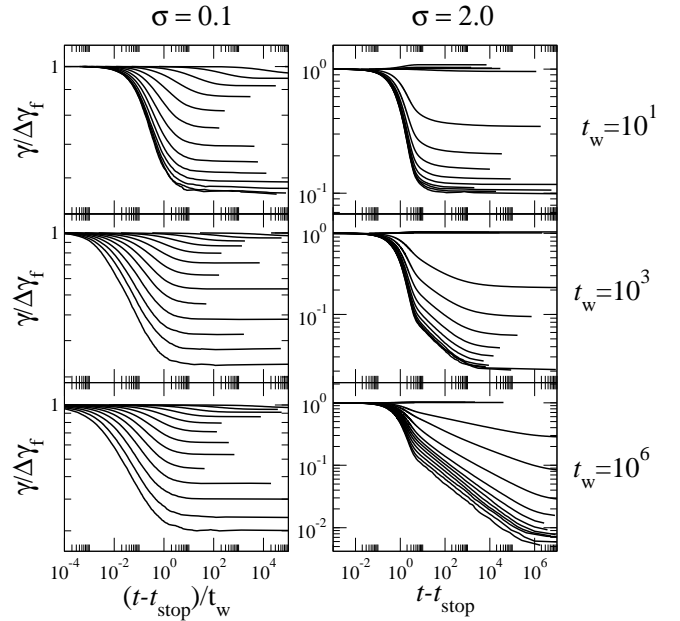


FIG. 6. Strain recovery as a function of the time since stress switch-off. The strain γ has been scaled by the forward plastic strain that arose while the stress was held imposed, $\Delta\gamma_f$. The scaled strain $\gamma/\Delta\gamma_f$ accordingly starts at unity at $t = t_{\text{stop}}^+$ (the forward and reverse elastic step strains at switch-on and switch-off having exactly cancelled each other). A full decay of $\gamma/\Delta\gamma_f \rightarrow 0$ as $t - t_{\text{stop}} \rightarrow \infty$ would indicate full strain recovery. Imposed stress prior to switch-off $\sigma_0 = 0.1$ and 2.0 in left and right panel columns respectively. Sample age prior to stress switch-on $t_w = 10^1, 10^3, 10^6$ in panels rows from top to bottom. Plastic forward strain accumulated prior to switch-off $\Delta\gamma_f = 0.001\sigma_0 \times (10.0/0.001)^{n/19}$ with $n = 5, 6 \dots$ in curves upwards in each panel.

more pronounced in younger samples (small t_w) for which group I elements are in relatively shallow traps and yield more rapidly.

For large $\Delta\gamma_f/\sigma_0$, such significant forward straining takes place before switch off, with significant flow for imposed stresses $\sigma_0 > \sigma_Y$, that the proportional degree of recovery post switch off is small. Accordingly, $\Delta\gamma_{\text{rec}}/\Delta\gamma_f \rightarrow 0$ as $\Delta\gamma_f/\sigma_0 \rightarrow \infty$, as indeed seen in Fig. 5.

We show finally in Fig. 6 the strain recovery as a function of the time $t - t_{\text{stop}}$ since switch-off. The six panels shown correspond to the smallest stress (left panel column) and largest stress (right panel column) and three different waiting times (increasing in panel rows downwards) for which the ultimate recovery in the limit $t - t_{\text{stop}} \rightarrow \infty$ is plotted versus the scaled forward strain $\Delta\gamma_f/\sigma_0$ in Fig. 5. Each panel in Fig. 6 shows results for the time dependent strain recovery for several different values of forward strain $\Delta\gamma_f$, increasing logarithmically in curves upwards, with the lowest curve in each panel of Fig. 6 corresponding to the leftmost datapoint in the counterpart curve of Fig. 5.

VI. CONCLUSIONS

In this work, we have studied theoretically recoverable and unrecoverable strain in amorphous and soft glassy materials such as dense foams and emulsions, glassy colloidal suspensions, jammed athermal suspensions, granular matter, and metallic and molecular glasses. Within the soft glassy rheology model [23, 24], we have simulated the rheological protocol in which a material of age t_w is subject to the switch-on at time zero of a shear stress of amplitude σ_0 , which is later switched off at some time t_{stop} , and the strain recovery observed as a function of the subsequent time $t - t_{\text{stop}}^+$.

We have reported the counter-intuitive phenomena that a significant component of the strain recovery post switch-off arises not via the recoil of elasticity, but instead by reverse plasticity. We have also showed that the time-evolution of strain post switch-off is not always monotonic, but can be non-monotonic (albeit in relatively rare parameter regimes): the plastic straining that takes place for times after switch-off $t > t_{\text{stop}}$ does not always occur in the negative direction, as in the initial elastic recoil at $t = t_{\text{stop}}$, but can sometimes in fact continue to accumulate in the same forward direction as the originally imposed stress. This provides a potential counterpart, in this imposed-stress protocol, to recent observations of non-monotonic stress relaxation after the switch off of an imposed strain [28–31].

We have discussed these observations in terms of the evolution of the SGR model’s population of elastoplastic elements. In particular, we have shown that strain recovery arises via elements that locally yielded during the initial forward plastic creep, resetting their local strains from positive values to zero as they did so. These elements then subsequently yield again post switch-off, resetting their local strains (and stresses) from negative values to zero. It is this plastic yielding from from negative to zero stress values that leads to global strain recovery, in order to maintain the global stress of the sample as a

whole equal to zero post switch-off.

The physics just described is strongly reminiscent of the concept of reversible plasticity, which has been studied extensively in the concept of oscillatory shear: localised plastic T1 events that arise in the forward direction during the positive part of a strain cycle exactly reverse during the reverse part of the cycle [34–42]. It should be noted, however, that the SGR model as studied here does not provide any spatial resolution of elemental positions. Accordingly, we are not able to make any statement as to whether a plastic event at a specific location later exactly reverses at the same location. Instead, we make only the weaker statement that some elements that yield during the initial forward creep later do so in reverse during recovery, recognising that our mean field approach does not track the spatial location of the elements. For this reason, we have chosen to use the weaker term *reverse* plasticity rather than the the term *reversible* plasticity. Future work should study creep and recovery in spatially resolved models, to establish a stronger link to reversible plasticity, with its precise connotations of elemental positions.

Related to this, we have assumed throughout that the shear remains macroscopically homogeneous across the sample, disallowing any possibility of shear band formation. However, it has been predicted that shear bands will tend to form in an imposed stress protocol at the end of any initial creep regime, as the strain rate dramatically increases and the sample yields [5]. This is likely to be an important effect for large values of $\Delta\gamma_f$ in particular. Future studies should consider extending this work to allow for the formation of shear bands.

Acknowledgements — The authors thank Mike Cates and Gareth McKinley for helpful comments on an early draft of the manuscript. We also thank Andrew Clarke for discussions and SLB (Schlumberger Cambridge Research Ltd.) for support. This project has received funding from the European Research Council (ERC) under the European Union’s Horizon 2020 research and innovation programme (grant agreement No. 885146).

-
- [1] Marcus Reiner, “Rheology,” in *Elasticity and Plasticity/Elastizität und Plastizität* (Springer, 1958) pp. 434–550.
- [2] K Weissenberg, “A continuum theory of rheological phenomena,” (1947).
- [3] James Lindsay White, “Considerations of unconstrained elastic recovery in viscoelastic fluids,” *Transactions of the Society of Rheology* **19**, 271–296 (1975).
- [4] AS Lodge, “A network theory of constrained elastic recovery in concentrated polymer solutions,” *Rheologica Acta* **1**, 158–163 (1958).
- [5] M Mooney, “The rhéology of raw rubber,” *Physics* **7**, 413–420 (1936).
- [6] M Reiner, “A classification of rheological properties,” *Journal of Scientific Instruments* **22**, 127 (1945).
- [7] Gavin J Donley, Piyush K Singh, Abhishek Shetty, and Simon A Rogers, “Elucidating the g” overshoot in soft materials with a yield transition via a time-resolved experimental strain decomposition,” *Proceedings of the National Academy of Sciences* **117**, 21945–21952 (2020).
- [8] Yul Hui Shim and Simon A Rogers, “Understanding the yielding behavior of graphene oxide colloids via experimental strain decomposition,” *Physics of Fluids* **35** (2023).
- [9] Krutarth Kamani, Gavin J Donley, and Simon A Rogers, “Unification of the rheological physics of yield stress fluids,” *Physical review letters* **126**, 218002 (2021).
- [10] Johnny Ching-Wei Lee, Katie M Weigandt, Elizabeth G Kelley, and Simon A Rogers, “Structure-property relationships via recovery rheology in viscoelastic materials,” *Physical review letters* **122**, 248003 (2019).
- [11] Thais C Brito-Oliveira, Izabel CF Moraes, Saman-

- tha C Pinho, and Osvaldo H Campanella, “Modeling creep/recovery behavior of cold-set gels using different approaches,” *Food Hydrocolloids* **123**, 107183 (2022).
- [12] Mathieu Leocmach, Christophe Perge, Thibaut Divoux, and Sébastien Manneville, “Creep and fracture of a protein gel under stress,” *Physical review letters* **113**, 038303 (2014).
- [13] Stefano Aime, Luca Cipelletti, and Laurence Ramos, “Power law viscoelasticity of a fractal colloidal gel,” *Journal of Rheology* **62**, 1429–1441 (2018).
- [14] Annemieke JW Ten Brinke, Louise Bailey, Henk NW Lekkerkerker, and Geoffrey C Maitland, “Rheology modification in mixed shape colloidal dispersions. part i: pure components,” *Soft Matter* **3**, 1145–1162 (2007).
- [15] Wilda Helen, Piero De Leonardis, Rein V Ulijn, Julie Gough, and Nicola Tirelli, “Mechanosensitive peptide gelation: mode of agitation controls mechanical properties and nano-scale morphology,” *Soft Matter* **7**, 1732–1740 (2011).
- [16] Pierre Lidon, Louis Villa, and Sébastien Manneville, “A mesoscale study of creep in a microgel using the acoustic radiation force,” *Soft matter* **15**, 2688–2702 (2019).
- [17] WC Tang, HZ Cui, and M Wu, “Creep and creep recovery properties of polystyrene aggregate concrete,” *Construction and Building Materials* **51**, 338–343 (2014).
- [18] Xuanhe Zhao, “Multi-scale multi-mechanism design of tough hydrogels: building dissipation into stretchy networks,” *Soft matter* **10**, 672–687 (2014).
- [19] Jeong-Yun Sun, Xuanhe Zhao, Widusha RK Illeperuma, Ovijit Chaudhuri, Kyu Hwan Oh, David J Mooney, Joost J Vlassak, and Zhigang Suo, “Highly stretchable and tough hydrogels,” *Nature* **489**, 133–136 (2012).
- [20] Shannon E Bakarich, Geoffrey C Pidcock, Paul Balding, Leo Stevens, Paul Calvert, *et al.*, “Recovery from applied strain in interpenetrating polymer network hydrogels with ionic and covalent cross-links,” *Soft Matter* **8**, 9985–9988 (2012).
- [21] Jiliang Hou, Xiuyan Ren, Shuang Guan, Lijie Duan, Guang Hui Gao, Yu Kuai, and Huixuan Zhang, “Rapidly recoverable, anti-fatigue, super-tough double-network hydrogels reinforced by macromolecular microspheres,” *Soft matter* **13**, 1357–1363 (2017).
- [22] Chris C Hornat and Marek W Urban, “Shape memory effects in self-healing polymers,” *Progress in Polymer Science* **102**, 101208 (2020).
- [23] Peter Sollich, François Lequeux, Pascal Hébraud, and Michael E Cates, “Rheology of soft glassy materials,” *Physical review letters* **78**, 2020 (1997).
- [24] Peter Sollich, “Rheological constitutive equation for a model of soft glassy materials,” *Physical Review E* **58**, 738 (1998).
- [25] Michael L Falk and James S Langer, “Deformation and failure of amorphous, solidlike materials,” *Annu. Rev. Condens. Matter Phys.* **2**, 353–373 (2011).
- [26] Chloe W Lindeman and Sidney R Nagel, “Multiple memory formation in glassy landscapes,” *Science Advances* **7**, eabg7133 (2021).
- [27] Alexandre Nicolas, Ezequiel E Ferrero, Kirsten Martens, and Jean-Louis Barrat, “Deformation and flow of amorphous solids: Insights from elastoplastic models,” *Reviews of Modern Physics* **90**, 045006 (2018).
- [28] Jan Hendricks, Ameer Louhichi, Vishal Metri, Rémi Fournier, Naveen Reddy, Laurent Bouteiller, Michel Cloitre, Christian Clasen, Dimitris Vlassopoulos, and WJ Briels, “Nonmonotonic stress relaxation after cessation of steady shear flow in supramolecular assemblies,” *Physical review letters* **123**, 218003 (2019).
- [29] Iana Sudreau, Mathilde Auxois, Marion Servel, Éric Lécolier, Sébastien Manneville, and Thibaut Divoux, “Residual stresses and shear-induced overaging in boehmite gels,” *Physical Review Materials* **6**, L042601 (2022).
- [30] Kieran A Murphy, Jonathon W Kruppe, and Heinrich M Jaeger, “Memory in nonmonotonic stress relaxation of a granular system,” *Physical Review Letters* **124**, 168002 (2020).
- [31] Rituparno Mandal, Diego Tapias, and Peter Sollich, “Memory in non-monotonic stress response of an athermal disordered solid,” *Physical Review Research* **3**, 043153 (2021).
- [32] Nathan C Keim, Joseph D Paulsen, Zorana Zeravcic, Srikanth Sastry, and Sidney R Nagel, “Memory formation in matter,” *Reviews of Modern Physics* **91**, 035002 (2019).
- [33] Guillemette Picard, Armand Ajdari, François Lequeux, and Lydéric Bocquet, “Elastic consequences of a single plastic event: A step towards the microscopic modeling of the flow of yield stress fluids,” *The European Physical Journal E* **15**, 371–381 (2004).
- [34] K Lawrence Galloway, Douglas J Jerolmack, and Paulo E Arratia, “Quantification of plasticity via particle dynamics above and below yield in a 2d jammed suspension,” *Soft Matter* **16**, 4373–4382 (2020).
- [35] Nathan C Keim and Paulo E Arratia, “Mechanical and microscopic properties of the reversible plastic regime in a 2d jammed material,” *Physical review letters* **112**, 028302 (2014).
- [36] Nathan C Keim and Paulo E Arratia, “Yielding and microstructure in a 2d jammed material under shear deformation,” *Soft Matter* **9**, 6222–6225 (2013).
- [37] Micah Lundberg, Kapilanjani Krishan, Ning Xu, Corey S O’Hern, and Michael Dennin, “Reversible plastic events in amorphous materials,” *Physical Review E* **77**, 041505 (2008).
- [38] Ido Regev, Turab Lookman, and Charles Reichhardt, “Onset of irreversibility and chaos in amorphous solids under periodic shear,” *Physical Review E* **88**, 062401 (2013).
- [39] Nikolai V Priezjev, “Reversible plastic events during oscillatory deformation of amorphous solids,” *Physical Review E* **93**, 013001 (2016).
- [40] Asaf Szulc, Muhittin Mungan, and Ido Regev, “Cooperative effects driving the multi-periodic dynamics of cyclically sheared amorphous solids,” *The Journal of Chemical Physics* **156** (2022).
- [41] Kentaro Nagasawa, Kunimasa Miyazaki, and Takeshi Kawasaki, “Classification of the reversible–irreversible transitions in particle trajectories across the jamming transition point,” *Soft matter* **15**, 7557–7566 (2019).
- [42] Kareem Khirallah, Botond Tyukodi, Damien Vandembroucq, and Craig E Maloney, “Yielding in an integer automaton model for amorphous solids under cyclic shear,” *Physical Review Letters* **126**, 218005 (2021).
- [43] Nathan C Keim and Joseph D Paulsen, “Multiperiodic orbits from interacting soft spots in cyclically sheared amorphous solids,” *Science Advances* **7**, eabg7685 (2021).
- [44] Muhittin Mungan and Thomas A Witten, “Cyclic an-

- nealing as an iterated random map,” *Physical Review E* **99**, 052132 (2019).
- [45] C Reichardt, Ido Regev, K Dahmen, S Okuma, and CJO Reichardt, “Perspective on reversible to irreversible transitions in periodic driven many body systems and future directions for classical and quantum systems,” arXiv preprint arXiv:2211.03775 (2022).
- [46] Suzanne M Fielding, Peter Sollich, and Michael E Cates, “Aging and rheology in soft materials,” *Journal of Rheology* **44**, 323–369 (2000).